Hindawi
International Journal of Energy Research
Volume 2023, Article ID 6659621, 10 pages
https://doi.org/10.1155/2023/6659621

Research Article

GLAD Fabricated Self-Powered Photodetector Based on WO_3 with SiO_2 as Interfacial Layer

Mir Waqas Alam,[1] **Ph. Nonglen Meitei**,[2] **Fatimah Saeed Aldughaylibi**,[1] **Amal BaQais**,[3] **Mir Waheed-Ur-Rehman**,[4] **Mohamad Akbar Ali**,[5,6] **and Christopher M. Maghanga**[7]

[1]*Department of Physics, College of Science, King Faisal University, Al-Ahsa 31982, Saudi Arabia*
[2]*Department of Electronics and Communication Engineering, National Institute of Technology, Nagaland 797103, India*
[3]*Department of Chemistry, College of Science, Princess Nourah Bint Abdulrahman University, Riyadh 11671, Saudi Arabia*
[4]*Nanoscience and Nano Technology Unit, Department of Physics, Islamia College of Science and Commerce, 11 Hawal, Srinagar, Jammu and Kashmir, India*
[5]*Department of Chemistry, College of Art and Science, Khalifa University of Science and Technology, PO Box 127788, Abu Dhabi, UAE*
[6]*Advanced Materials Chemistry Center (AMCC), Khalifa University of Science and Technology, PO Box 127788, Abu Dhabi, UAE*
[7]*Department of Biological & Physical Sciences, Kabarak University, Private Bag-20157, Kabarak, Kenya*

Correspondence should be addressed to Mir Waqas Alam; wmir@kfu.edu.sa
and Christopher M. Maghanga; cmaghanga@kabarak.ac.ke

Received 8 June 2023; Revised 5 September 2023; Accepted 5 October 2023; Published 19 October 2023

Academic Editor: Soumyendu Roy

Photodetectors based on one-dimensional structures have recently attracted great interest due to their high surface-to-volume ratio and light-trapping efficiency. In this study, a self-powered photodetector based on vertically aligned WO_3 nanorod with SiO_2 as an interfacial layer has been fabricated using glancing angle deposition. Scanning electron microscope (SEM) analysis confirms the successful growth of WO_3 nanorod and SiO_2 thin film with a thickness of ~125 nm and ~70 nm, respectively. The device's optical properties were also analysed using UV-visible spectroscopy, which revealed a wide bandgap and an intense absorption peak in the ultraviolet region. The electrical analysis showed a nonlinear rectifying current-voltage behaviour with high photosensitivity. Additionally, the photodetector exhibits a fast response of 0.31 s rise time and 0.32 s fall time at 0 V. Moreover, the devices possess a high detectivity and a responsivity of 0.68 mA/W. Thus, the obtained finding reveals a potential candidate for self-powered photodetector application.

1. Introduction

In recent years, metal oxide one-dimensional (1D) nanostructures, including nanowires (NW) and nanorods (NR), have gained significant attention in the field of electronics and optoelectronics due to their unique combination of electrical, optical, and structural properties, such as a high surface-to-volume ratio and tunable electrical and optical properties [1–3]. These properties make 1D structures suitable for various applications such as energy conversion and storage, sensing, and optoelectronics [3–6]. 1D self-powered devices using various techniques and materials, such as V_2O_5 [7–9] and InN [10, 11], are already reported. Among the commonly used metal oxide such as TiO_2, ZnO, NiO_2, Gd_2O_3, and Ga_2O_3 [12–17] for the study of optoelectronics, tungsten oxide (WO_3) is a promising candidate for the construction of high-performance ultraviolet (UV) photodetectors due to its high bandgap with good chemical and physical properties [18]. Among the wide variety of photodetector structures reported, a metal semiconduction (MS) junction is widely used due to its ease of preparation. Studies have shown that an MS-based photodetector is an effective method to produce a comparable performance that facilitates photogenerated electron-hole at the interface of the junction [19, 20]. However, the MS-

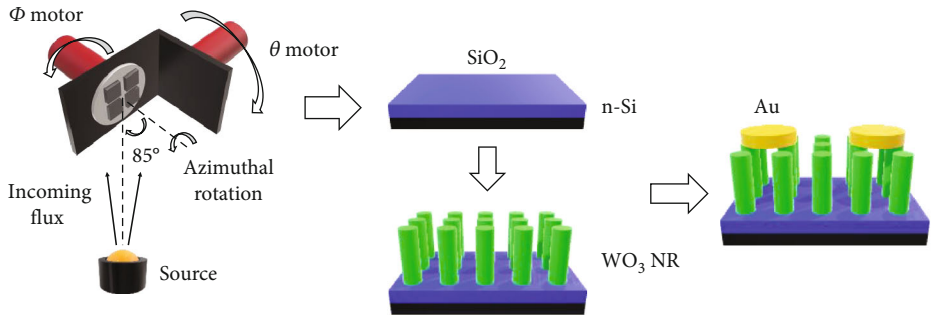

Figure 1: Schematic illustrations showing Au/WO_3/SiO_2 HS via GLAD technique.

based photodetector structure also faced a problem of slow responses due to its photoconductive effect [21]. In recent years, numerous researchers have focused on improving the performance of devices based on WO_3 nanostructures. For instance, a study on WO_3 NW by Rajkumari and Singh performed annealing to reduce the device defect and improve the device response time (rise time/fall time) from 1.78 s/1.09 s to 1.33 s/0.94 s [18]. Another study by Rajkumari et al. showed improved photoresponse (rise time/fall time) of 0.84 s/0.78 s after incorporating Ag nanoparticles on top of WO_3 NW [22]. In order to enhance the device's performance further, an updated model of metal semiconduction with an interfacial layer is introduced. The introduction of the interfacial layer strongly impacts the device's photoconductive characteristics. Studies have shown that adding an interfacial layer enhances the response speed of the photodetector [23]. Among the existing materials for the use of interfacial layer, SiO_2 is a highly suitable material due to its low cost, ease of manufacture, and high chemical stability [24].

In this study, our primary objective is to investigate the effects of inserting a SiO_2 interfacial layer between n-Silicon (Si) and WO_3 NR in a hybrid structure (HS) UV photodetector. We aim to comprehensively analyse how this interfacial layer influences the photoconductive properties of the photodetector, specifically focusing on its impact on response speed and overall efficiency. By fabricating the HS using glancing angle deposition (GLAD), we intend to uncover insights into the performance enhancement achievable through configuration. GLAD, known for its precision in controlling nanostructured film growth, allows us to tailor the morphology and properties of the WO_3 NR layer in our hybrid structure. Ultimately, this research is aimed at contributing to advancing photodetector technology by paving the way for developing high-performance devices with enhanced response capabilities for various applications. Further, Keithley 4200 scs and monochromator (New Port TLS-300XU) were used to analyse the device's current (I)–voltage (V) characteristics. Finally, our fabricated HS photodetector showed enhanced photosensitivity and fast response with a self-powered ability.

2. Experimental Details

The WO_3/SiO_2 HS was prepared using n-type silicon (Si) substrate (resistivity of 1-10 ohm-cm with $525 \pm 25\,\mu$m thickness, Ultra nanotech) with an electron beam (e-beam) evaporation technique and a glancing angle deposition technique. Before the SiO_2 thin film (TF) deposition, the Si substrate was ultrasonically cleaned (MTI, KJ Group) with acetone, methanol, and deionized water for 3 min. After that, a SiO_2 (99.99% purity, Ultra nanotech) TF of 70 nm was deposited on top of the Si substrate. For the deposition of WO_3 NR, the substrate was kept at 85° normal to the crucible containing WO_3 granule of 99.99% purity (Ultra nanotech). The deposition was carried out with a base pressure of $\sim 5 \times 10^{-6}$ mbar, and the substrate was azimuthally rotated at 30 rpm with a constant deposition rate of 1 Å/s. Figure 1 illustrates the schematic representation of the GLAD model. It comprises two motors: the ϕ motor, responsible for executing azimuthal rotations, and the θ motor, regulating the angle formed between the substrate's normal and the incident flux. By employing these motors, alterations to the structural configuration can be achieved. For thin film deposition, the angle θ is kept at 0°. Afterward, the angle θ is changed to 85° along with the rotation of the substrate azimuthally at a constant speed for the growth of vertical nanocolumnar structure. During the growth of vertical nanoclumnar structure, the incident flux (F) can be divided into two components: a lateral component denoted as $F_{\parallel} = F \sin\theta$ and a vertical component denoted as $F_{\perp} = F \cos\theta$. As the substrate maintains a consistent rotational pace, particles are uniformly deposited onto it from the $F_{\parallel}$ component. However, over the course of a full revolution, the cumulative effect of $F_{\parallel}$ cancels out due to opposing directions. This outcome results in the prominence of the vertical growth influenced by the $F_{\perp}$ component. Finally, gold (Au) contact of 0.1 cm diameter (area = 7.85×10^{-3} cm^2) was deposited on top of WO_3 NR to form the Schottky contact.

3. Results and Discussion

3.1. Optical Analysis. The UV-Vis spectra of the WO_3/SiO_2 HS were recorded using UV-Vis spectrophotometer (Hitachi UH4150) as shown in Figure 2(a). The spectra reveal a strong absorption in the UV region. The maximum absorption in the UV region can be ascribed to the band-to-band transition of WO_3 and SiO_2 [25–27]. A broad peak in the absorption above 400 nm was also observed. This absorption can be attributed to oxygen vacancies creating a midgap state

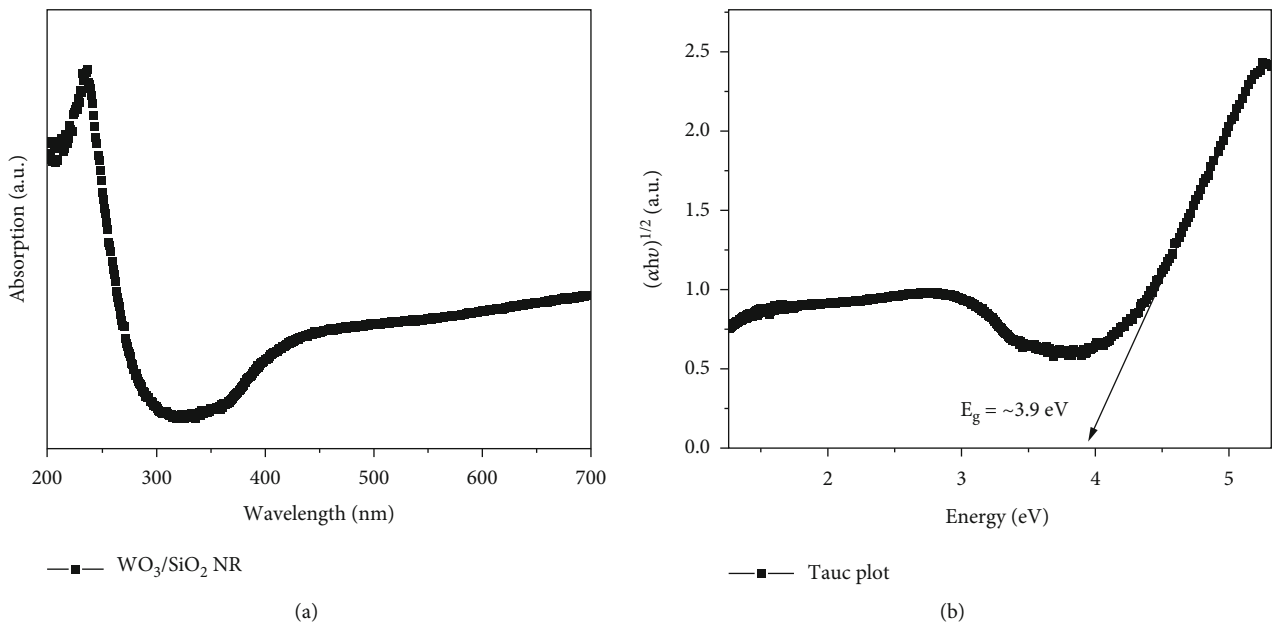

Figure 2: (a) Absorption spectra and (b) the Tauc plot of WO_3/SiO_2 HS.

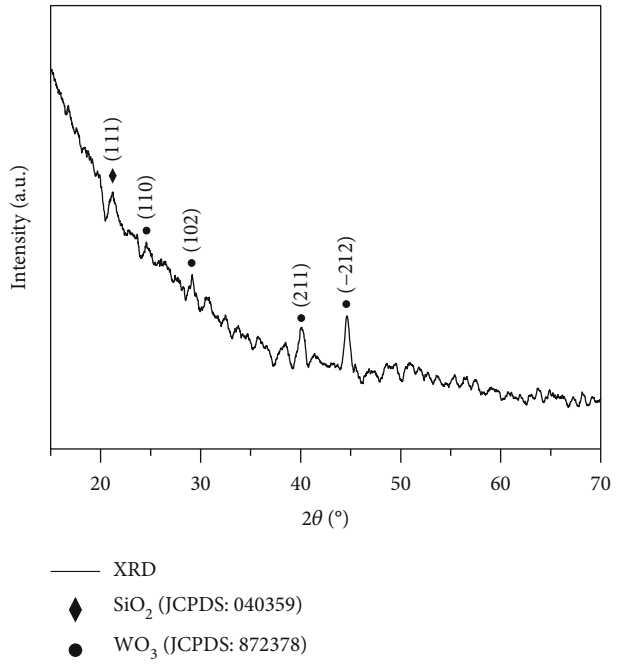

Figure 3: XRD pattern of WO_3/SiO_2 HS.

within the bandgap [28]. Further, the optical bandgap (E_g) for the HS was calculated using the Tauc plot [29] given by

$$\alpha h\upsilon \, \alpha \left(h\upsilon - E_g\right)^{1/n}, \tag{1}$$

where α = absorption coefficient, $h\upsilon$ = photon energy, and n = ½ for indirect transition. By extrapolating $(\alpha h\upsilon)^2 = 0$, as shown in Figure 2(b), the bandgap was obtained as ~3.9 eV.

3.2. Structural Analysis. Figure 3 shows the X-ray diffraction (XRD) pattern of WO_3/SiO_2 HS obtained using a Rigaku X-ray diffractometer from 15° to 80° with a scan rate of 0.02 °/s. The diffraction peak was indexed as (110), (102), (211), and (-212) plane, displaying a WO_3 monoclinic NR structure with JCPDS: 872378. Also, a peak with (111) plane was observed corresponding to the SiO_2 cubic structure. In addition, the distinct peak observed in the XRD pattern confirms the polycrystalline nature of the as-grown WO_3/SiO_2 HS.

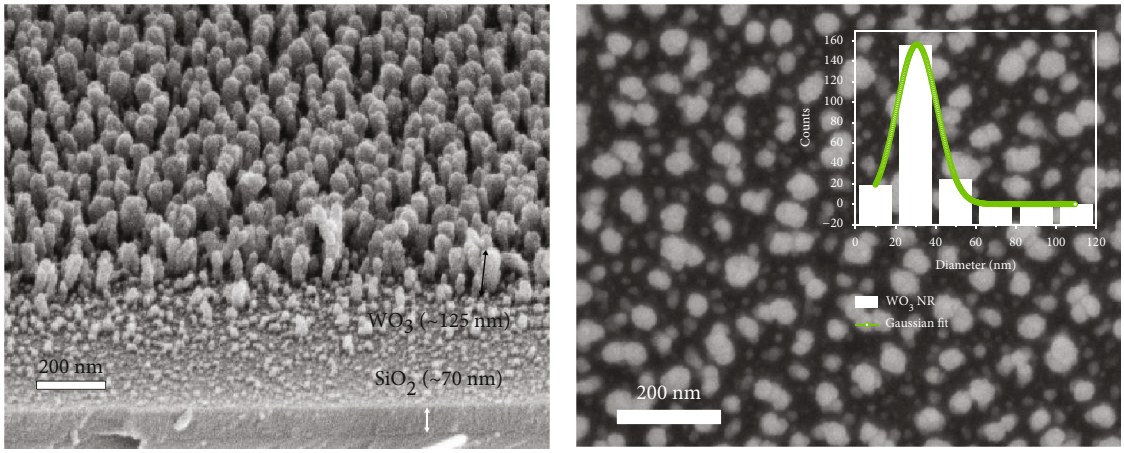

(a) (b)

Figure 4: (a) Cross-sectional view and (b) top view. Inset: diameter histogram with Gaussian fitting of WO_3 NR.

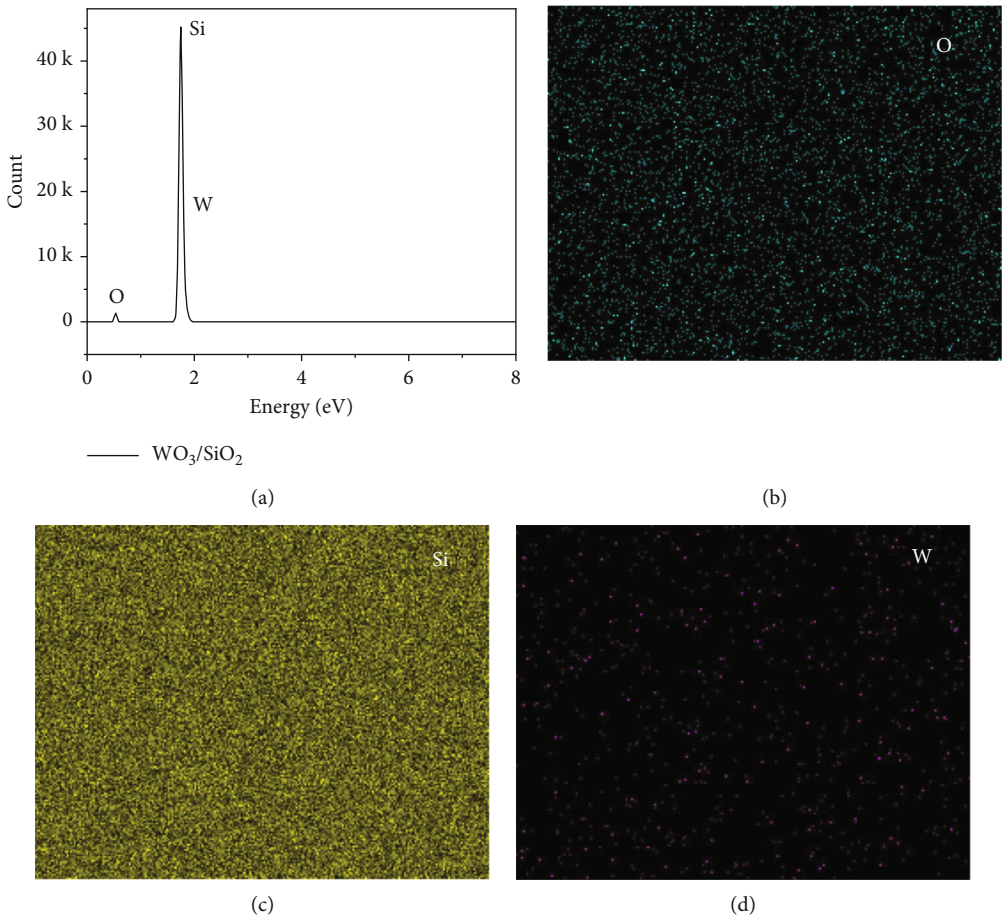

(a) (b) (c) (d)

Figure 5: (a) EDS spectrum of WO_3/SiO_2 HS and (b–d) elemental mapping of O, Si, and W.

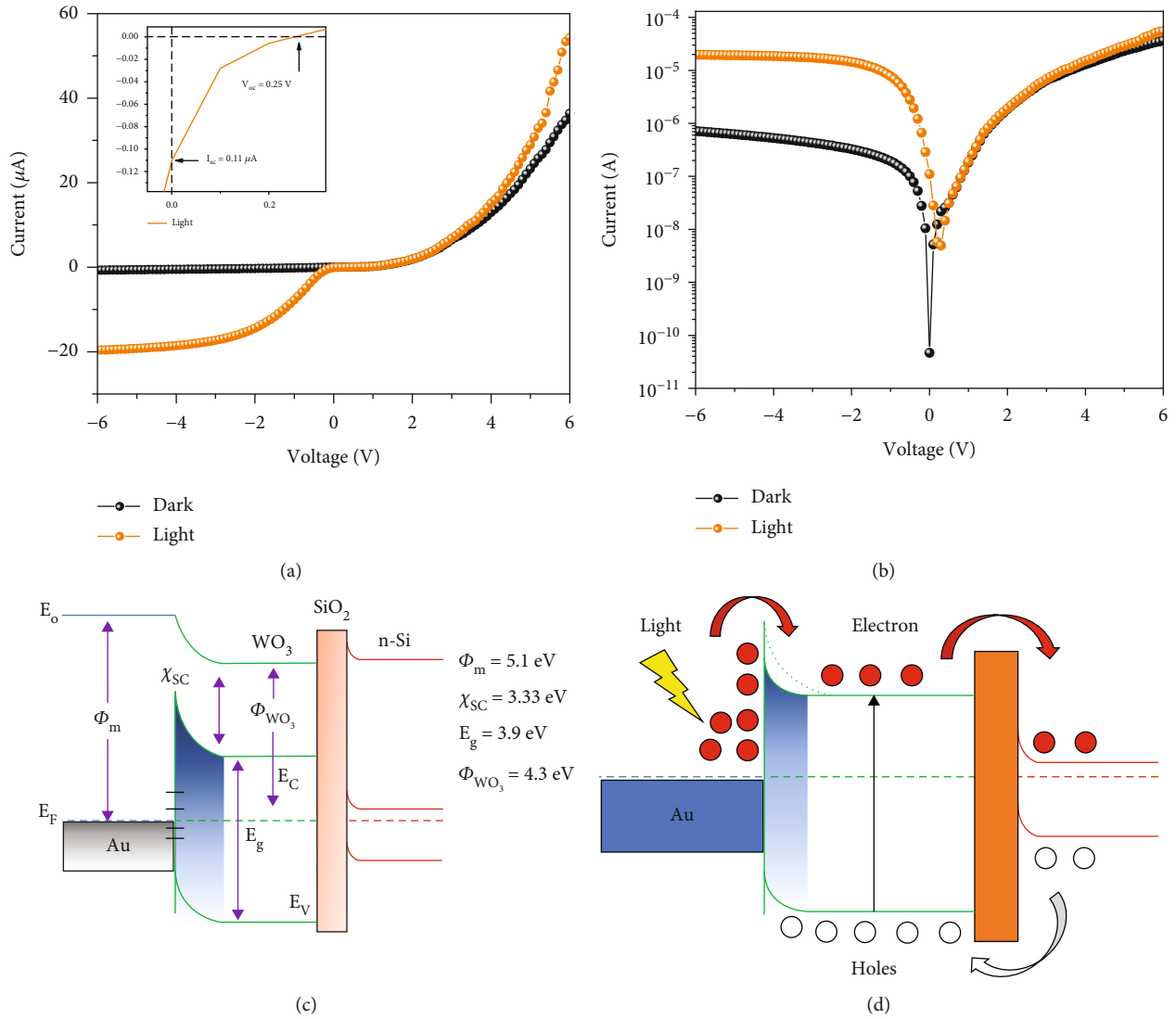

FIGURE 6: (a) WO_3/SiO_2 HS photodetector I-V characteristics. Inset: showing V_{oc} and I_{sc}. (b) I-V in log. (c) Energy band diagram under dark. (d) Energy band diagram under the light.

The average crystallite size was calculated from the WO_3 NR peak by employing Scherrer's equation [30] as follows:

$$D = \frac{0.9\lambda}{\beta \cos\theta}, \tag{2}$$

where $\lambda = 1.5406$ Å is the wavelength of the incident X-rays, β is the FWHM, θ is the Bragg diffraction angle, and D is the average crystallite size. The average crystallite was found to be 11.18 nm along with a dislocation density (δ) of 7.99×10^{15} lines/m^2 calculated using the equation given by Hassan et al. [31].

The cross-sectional Field Emission Scanning Electron Microscope (FESEM) image was performed using Zeiss Sigma, NIT Durgapur, as shown in Figure 4(a). The cross-sectional image confirms the successful growth of the SiO_2 TF and WO_3 NR. A uniform structure with a thickness of 70 nm for SiO_2 and 125 nm for WO_3 was obtained. Figure 4(b) shows the top view FESEM image of the WO_3 NR. It can be seen that the as-grown NR are densely packed with fully grown WO_3 NR. Some undergrown NR are also visible along with the fully grown WO_3 NR due to the shadowing effect associated with the GLAD technique [32]. Further, the average particle size of the WO_3 NR was obtained as ~25 nm, as shown in Figure 4(b) inset. In addition, energy-dispersive X-ray spectroscopy (EDS) analysis was used to determine the purity and the presence of W, Si, and O in the sample. Figures 5(a)–5(d) shows the EDS spectrum and elemental mapping of WO_3/SiO_2. It can be seen that the elements of W, Si, and O are uniformly distributed in the as-grown sample.

3.3. Electrical Analysis. Figures 6(a) and 6(b) show the I-V linear and log scale of WO_3/SiO_2 HS PD under dark and light conditions using xenon light with an intensity of 2.5 mW/cm^2. The device displayed rectifying characteristics under a biasing voltage of -6 V to 6 V, indicating the

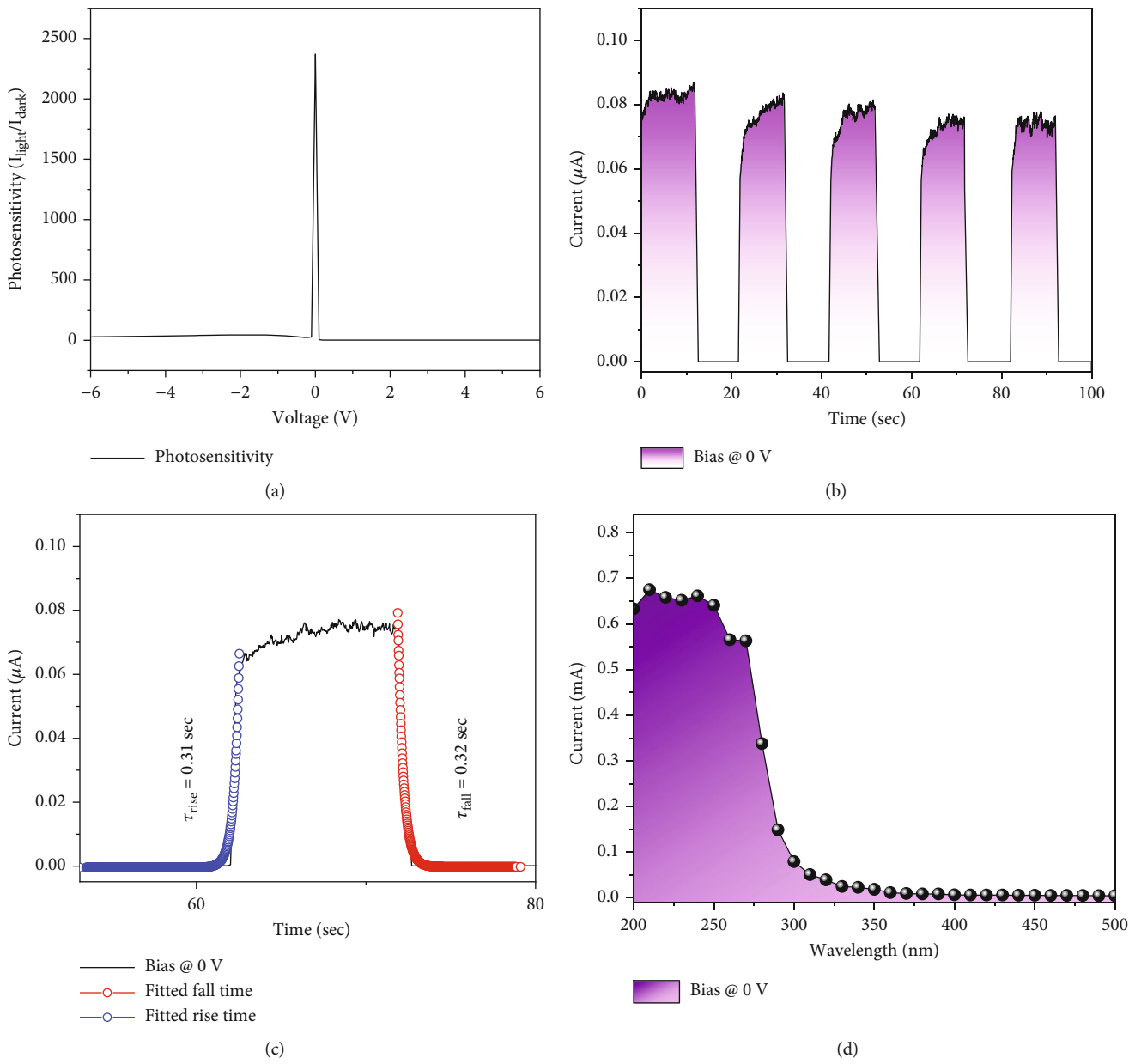

Figure 7: Continued.

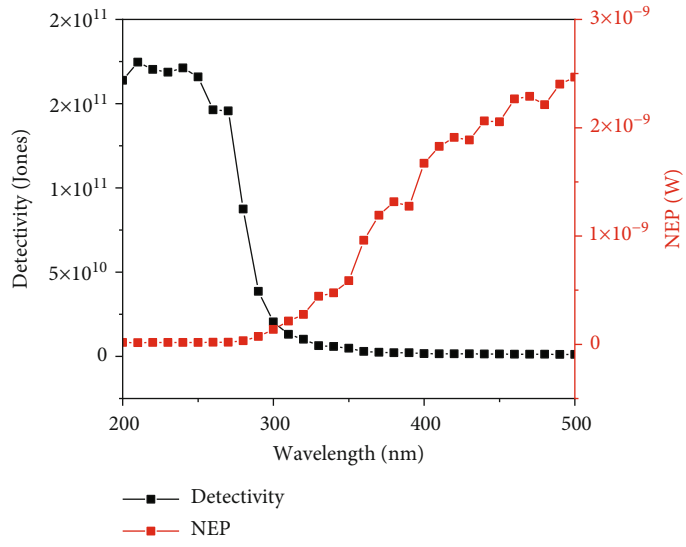

FIGURE 7: (a) Photosensitivity, (b) switching response under light and dark, (c) rise/fall time fitting, (d) responsivity, and (e) detectivity and NEP of WO_3/SiO_2 HS photodetector.

formation of a good Schottky junction between the Au electrode and the WO_3 NR. For nonideal Schottky diodes with a series resistance, it is assumed that the total current flowing through the device is primarily attributed to the thermionic emission (TE) current given by [33]

$$I = I_o\left[\exp\left(\frac{qV}{nkT}\right) - 1\right], \tag{3}$$

$$I_o = AA^*T^2 \exp\left(\frac{-q\phi_b}{kT}\right), \tag{4}$$

where T, q, V, n, k, I_o, A, A^*, and ϕ_b represent the temperature (300 K), the electron charge, the biasing voltage, the ideality factor, the Boltzmann constant, the saturation current at reverse bias, the area of the contact, the Richardson constant ($112\,\mathrm{Acm^{-2}K^{-2}}$ for n-type Si), and effective barrier height, respectively. The value of ϕ_b under dark and light conditions using equation (4) was obtained as 0.78 eV and 0.70 eV. The interfacial layer of SiO_2 acts as a tunnel barrier that does not hinder electron flow at low voltages. Therefore, the as-grown device exhibits a very low dark current of ~46 pA due to the effect of the SiO_2 layer [23] and photocurrent of ~0.11 μA at 0 V, respectively. In addition, the device displayed photovoltaic characteristics with an open voltage (V_{oc}) of 0.25 V and short-circuit current (I_{sc}) of 0.11 μA, as shown in Figure 6(a) inset.

The mechanism of the WO_3/SiO_2 HS photodetector can be comprehended with the help of an energy band diagram, as illustrated in Figures 6(c) and 6(d). Surface states frequently influence the performance of optoelectronic responses. These surface properties give rise to a phenomenon where the upward band undergoes a bending effect close to the surface, thereby capturing and trapping holes. Under dark conditions, oxygen molecules (O_2) from the atmosphere get absorbed on WO_3 NR. These O_2 react with the electron (e^-) from the conduction band and form adsorbed oxygen ions ($O_2 + e^- \longrightarrow O_2^-$). These ionized oxygen at the Au and WO_3 NR interface forms a thin depletion layer with low conductivity [34], as shown in Figure 6(c). Under light conditions, the photon energy excites the electrons from the valence band to the conduction band; as a result, more electron-hole pairs are generated in the device. The adsorbed ionized oxygen traps the photogenerated holes at the surface of WO_3 NR, thereby releasing the oxygen through the desorption process ($O_2^- + h^+ \longrightarrow O_2$). As a result, the depletion zone becomes narrower and reduces the band bending, causing an increased conductivity (Figure 6(d)). However, the recombination of the electrons and holes can limit the response time of the photodetector. Therefore, adding a SiO_2 interfacial layer between WO_3 and Si substrate improved the device insulation as SiO_2 will act as the electrical insulator. This improved insulation reduces the charge carrier recombination rate, increasing the number of available charge carriers for conduction [23]. As a result, the response time of the photodetector is reduced.

In addition, the devices showed high photosensitivity (I_L/I_D) of ~2371 at 0 V, as shown in Figure 7(a). Other crucial parameters for testing the photodetector's capabilities, such as photoswitching and photoresponsivity, were also performed. Figure 7(b) shows the photoswitching of the WO_3/SiO_2 HS PD at 0 V. It can be seen that the device exhibits a good stability switching response with two distinct states revealing the response and recovery speed of the device. To calculate the rise time ($I(t)_r$) and fall time ($I(t)_f$) of the device, fitting was performed with the following equations (5) and (6) on the switching response at 0 V.

$$I(t)_r = I_d + A\exp\left(\frac{t}{\tau_r}\right), \tag{5}$$

Table 1: Comparison of the characteristic parameters with existing photodetectors.

Materials	Voltages (V)	Rise time/fall time (s)	R (mA/W)	D^* (Jones)	Ref.
$Au/WO_3/SiO_2/Si$	0	0.31/0.32	0.68	1.74639×10^{11}	This work
WO_3/Si	3	1.78/1.09	9.66 x 10^3	5.94×10^{12}	[18]
β-Ga_2O_3/NiO	0	0.01/0.008	0.245	0.181×10^9	[36]
SnO_2 nanowire	0	0.72/1.78	0.36	3.02×10^9	[37]

$$I(t)_f = I_d + A \exp\left(\frac{-t}{\tau_f}\right), \tag{6}$$

where $I(t)_r$ and $I(t)_f$ are the photocurrent time, I_d is the dark current, A is the scaling constant, and τ_r and τ_f are the rise and fall time. From Figure 7(c), the rise time of 0.31 s and fall time of 0.32 s were obtained from the fitted curve. The obtained result significantly outperformed the previously reported PD device using WO_3 [18, 22]. The existence of SiO_2 as an interfacial layer significantly improves the device's response speed. Finally, the responsivity of the device at 0 V was calculated using the following [35]:

$$R = \frac{I_p}{P_{\text{in}}}, \tag{7}$$

where I_p is the photocurrent and P_{in} is the power of incident light. The calculated value of R is plotted as shown in Figure 7(d). The device exhibits a larger photocurrent response in the UV region and lower as its wavelength increases, indicating a good spectrum selectivity response. To validate the detection of signal in a noise environment, the detectivity (D^*) and noise equivalent power (NEP) was calculated using the following [35]:

$$D^* = \frac{R_\lambda}{(2XeXI_d)^{1/2}}, \qquad \text{NEP} = \frac{(AXB)^{1/2}}{D^*}, \tag{8}$$

where R_λ is the responsiveness, e is the charge of the electron, A is the effective area of radiation of the photodetector, and B is taken as 1 KHz bandwidth for flicker noise. The calculated D^* and NEP were plotted as shown in Figure 7(e). Table 1 shows the comparison of our work with the existing reported literature. Our device exhibits an excellent ability to detect weak signals from the noise environment.

4. Conclusion

In summary, this study successfully demonstrated the WO_3/SiO_2 HS photodetector fabrication using a glancing angle deposition technique incorporated inside an e-beam evaporator. The optical analysis confirmed a strong absorption in the UV region with a bandgap of ~3.9 eV. This underscores its potential for applications requiring sensitivity to ultraviolet light, such as UV photodetectors and sensors. As confirmed by SEM and EDS analysis, the successful growth of distinct WO_3 NR and SiO_2 TF underpins the precisely tuned and controlled deposition process. The electrical analysis of the WO_3/SiO_2 HS device revealed a self-powered characteristic with $V_{\text{oc}} = 0.25$ V and $I_{\text{sc}} = 0.11\ \mu$A. In addition, the device showed high photosensitivity and fast switching response of rise/fall time of 0.31 s/0.32 s at 0 V. Further, our device also displayed high responsivity of 0.68 mA/W with low NEP and high detectivity. These results demonstrate a cost-effective and easy fabrication way of improving the device performance by adding an interfacial layer.

Data Availability

The datasets used and/or analysed during the current study are available from the corresponding authors upon reasonable request.

Conflicts of Interest

The authors declare no conflict of interest.

Authors' Contributions

We confirm that all listed authors have made a significant scientific contribution to the research in the manuscript, approved its claims, and agreed to be the authors of this manuscript. We declare that no further changes to authorship will be made after this point.

Acknowledgments

This work was supported by the Deanship of Scientific Research, Vice Presidency for Graduate Studies and Scientific Research, King Faisal University, Saudi Arabia (Project No: GRANT4,408). The authors would like to acknowledge Princess Nourah bint Abdulrahman University Researchers Supporting Project number (PNURSP2023R230), Princess Nourah bint Abdulrahman University, Riyadh, Saudi Arabia.

References

[1] P. N. Meitei and N. K. Singh, "Annealing effect on structural and optical properties of glad synthesized Gd2O3 nanorod," *Discover Materials*, vol. 3, no. 1, p. 3, 2023.

[2] N. M. Devi, A. BaQais, A. K. Debnath, M. W. Alam, and N. K. Singh, "Improved photodetection capabilities of Ag@CeO2 Nanorod composite array using GLAD technique," *Ceramics International*, vol. 48, no. 20, pp. 30107–30117, 2022.

[3] P. Nonglen Meitei and N. K. Singh, "Effect of annealing on forming-free bipolar resistive switching of Gd2O3 thin films," *Journal of Alloys and Compounds*, vol. 941, p. 168900, 2023.

[4] M. Nehra, N. Dilbaghi, G. Marrazza et al., "1D semiconductor nanowires for energy conversion, harvesting and storage applications," *Nano Energy*, vol. 76, p. 104991, 2020.

[5] P. N. Meitei, B. Moirangthem, C. Ngangbam, M. W. Alam, and N. K. Singh, "Investigation on structural and photodetection properties of Gd2O3 thin films after annealing," *Journal of Materials Science: Materials in Electronics*, vol. 33, no. 14, pp. 10705–10714, 2022.

[6] B. Moirangthem, P. N. Meitei, A. K. Debnath, and N. K. Singh, "Forming-free RRAM device based on HfO2 thin film for non-volatile memory application using E-beam evaporation method," *Journal of Materials Science: Materials in Electronics*, vol. 34, no. 4, p. 306, 2023.

[7] S. Shafique, S. Yang, Y. Wang, Y. T. Woldu, B. Cheng, and P. Ji, "High-performance photodetector using urchin-like hollow spheres of vanadium pentoxide network device," *Sensors and Actuators A: Physical*, vol. 296, pp. 38–44, 2019.

[8] S. Shafique, S. Yang, Y. T. Woldu, and Y. Wang, "Hierarchical synthesis of urchin-like V2O5 hollow spheres and its photodetection properties," *Sensors and Actuators A: Physical*, vol. 288, pp. 107–116, 2019.

[9] S. Shafique, S. Yang, T. Iqbal et al., "Improving the performance of V2O5/rGO hybrid nanocomposites for photodetector applications," *Sensors and Actuators A: Physical*, vol. 332, p. 113073, 2021.

[10] A. Imran, M. Sulaman, S. Yang et al., "Molecular beam epitaxy growth of high mobility InN film for high-performance broadband heterointerface photodetectors," *Surfaces and Interfaces*, vol. 29, p. 101772, 2022.

[11] A. Imran, M. Sulaman, M. Yousaf et al., "Growth of high mobility InN film on Ga-polar GaN substrate by molecular beam epitaxy for optoelectronic device applications," *Advanced Materials Interfaces*, vol. 10, no. 20, article 2200105, 2023.

[12] B. D. Boruah, A. Mukherjee, S. Sridhar, and A. Misra, "Highly dense ZnO nanowires grown on graphene foam for ultraviolet photodetection," *ACS Applied Materials & Interfaces*, vol. 7, no. 19, pp. 10606–10611, 2015.

[13] P. Pooja and P. Chinnamuthu, "Annealed n-TiO2/In2O3 nanowire metal-insulator-semiconductor for highly photosensitive low-noise ultraviolet photodetector," *Journal of Alloys and Compounds*, vol. 854, p. 157229, 2021.

[14] L. T. Chanu and N. K. Singh, "Fast response photodetector analysis based on NiO nanowire using a catalyst-free technique," *Applied Physics A: Materials Science & Processing*, vol. 128, no. 11, p. 993, 2022.

[15] P. N. Meitei, M. W. Alam, C. Ngangbam, and N. K. Singh, "Enhanced UV photodetection characteristics of annealed Gd2O3 nanorods," *Applied Nanoscience*, vol. 11, no. 4, pp. 1437–1445, 2021.

[16] M. W. Alam, Z. Wang, S. Naka, and H. Okada, "Performance enhancement of top-contact pentacene-based organic thin-film transistors with bilayer WO_3/Au electrodes," *Japanese Journal of Applied Physics*, vol. 52, article 03BB08, 2013.

[17] S. R. Meitei, R. Rajkumari, and N. K. Singh, "Post deposition annealing effect on the electrical properties of β-Ga2O3 nanowire," *Journal of Materials Science: Materials in Electronics*, vol. 31, no. 22, pp. 20378–20386, 2020.

[18] R. Rajkumari and N. K. Singh, "Effect of annealing on the structural and electrical properties of GLAD synthesized vertical aligned WO3 nanowire," *IEEE Transactions on Nanotechnology*, vol. 18, pp. 676–683, 2019.

[19] H. Qiao, Z. Huang, X. Ren et al., "Self-powered photodetectors based on 2D materials," *Advanced Optical Materials*, vol. 8, no. 1, article 1900765, 2020.

[20] J. Meng and Z. Li, "Schottky-contacted nanowire sensors," *Advanced Materials*, vol. 32, no. 28, p. 2000130, 2020.

[21] X. Yan, X. Ji, J. Wang et al., "Improve photo-to-dark current ratio of $_{p\text{-}Si/SiO2/n\text{-}Ga2O3}$ heterojunction solar-blind photodetector by inserting $_{SiO2}$ barrier layer," *Journal of Vacuum Science & Technology B*, vol. 40, no. 5, article 052207, 2022.

[22] R. Rajkumari, C. Ngangbam, and N. K. Singh, "High detectivity photodetector based on WO3 nanowires by the surface plasmonic effect of Ag nanoparticles," *IEEE Electron Device Letters*, vol. 43, no. 3, pp. 470–473, 2022.

[23] H. Kim, M. D. Kumar, and J. Kim, "Highly-performing Ni/SiO2/Si MIS photodetector for NIR detecting applications," *Sensors and Actuators A: Physical*, vol. 233, pp. 290–294, 2015.

[24] D. Yang, Y. Ren, F. Du et al., "Enhanced response speed of TiO2 nanoarrays based all solid-state ultraviolet photodetector via SiO2 dielectric layer," *Journal of Alloys and Compounds*, vol. 867, p. 159053, 2021.

[25] M. Schieder, T. Lunkenbein, T. Martin, W. Milius, G. Auffermann, and J. Breu, "Hierarchically porous tungsten oxide nanotubes with crystalline walls made of the metastable orthorhombic polymorph," *Journal of Materials Chemistry A*, vol. 1, no. 2, pp. 381–387, 2013.

[26] P. J. Boruah, R. R. Khanikar, and H. Bailung, "Synthesis and characterization of oxygen vacancy induced narrow bandgap tungsten oxide (WO3−x) nanoparticles by plasma discharge in liquid and its photocatalytic activity," *Plasma Chemistry and Plasma Processing*, vol. 40, no. 4, pp. 1019–1036, 2020.

[27] J. Wang, Q. Ran, X. Xu, B. Zhu, and W. Zhang, "Preparation and optical properties of TiO_2-SiO_2 thin films by sol-gel dipping method," *IOP Conference Series: Earth and Environmental Science*, vol. 310, article 042029, 2019.

[28] Q. Liu, F. Wang, H. Lin et al., "Surface oxygen vacancy and defect engineering of WO3 for improved visible light photocatalytic performance," *Catalysis Science & Technology*, vol. 8, no. 17, pp. 4399–4406, 2018.

[29] P. Makuła, M. Pacia, and W. Macyk, "How to correctly determine the band gap energy of modified semiconductor photocatalysts based on UV–Vis spectra," *Journal of Physical Chemistry Letters*, vol. 9, no. 23, pp. 6814–6817, 2018.

[30] A. Patterson, "The Scherrer formula for X-ray particle size determination," *Physical Review*, vol. 56, no. 10, pp. 978–982, 1939.

[31] M. Hassan, S. Younas, F. Sher, S. S. Husain, S. Riaz, and S. Naseem, "Room temperature ferromagnetism in single-phase Zn1−x Mn x S diluted magnetic semiconductors fabricated by co-precipitation technique," *Applied Physics A: Materials Science and Processing*, vol. 123, no. 5, pp. 1–8, 2017.

[32] Y. Zhao, D. Ye, G.-C. Wang, and T.-M. Lu, *Designing nanostructures by glancing angle deposition*, A. Lakhtakia and S. Maksimenko, Eds., SPIE, San Diego, California, USA, 2003.

[33] M. Yilmaz, Y. Demir, S. Aydogan, and M. L. Grilli, "Density functional theory calculations of Pinus brutia derivatives and its response to light in a Au/n-Si device," *Energies*, vol. 14, no. 23, p. 7983, 2021.

[34] P. Sharma, K. Sreenivas, and K. V. Rao, "Analysis of ultraviolet photoconductivity in ZnO films prepared by unbalanced magnetron sputtering," *Journal of Applied Physics*, vol. 93, no. 7, pp. 3963–3970, 2003.

[35] A. Rasool, M. C. Santhosh Kumar, M. H. Mamat, C. Gopalakrishnan, and R. Amiruddin, "Analysis on different detection mechanisms involved in ZnO-based photodetector and photodiodes," *Journal of Materials Science: Materials in Electronics*, vol. 31, no. 9, pp. 7100–7113, 2020.

[36] J. Yu, M. Yu, Z. Wang et al., "Improved photoresponse performance of self-powered β-Ga_2O_3/NiO heterojunction UV photodetector by surface plasmonic effect of Pt nanoparticles," *IEEE Transactions on Electron Devices*, vol. 67, no. 8, pp. 3199–3204, 2020.

[37] P. Chetri and J. C. Dhar, "Self-powered UV detection using SnO2 nanowire arrays with Au Schottky contact," *Materials Science in Semiconductor Processing*, vol. 100, pp. 123–129, 2019.